Published in final edited form as:
Cancer Res. 2014 September 15; 74(18): 5079–5090. doi:10.1158/0008-5472.CAN-14-1203.

Natural Killer Cells Eradicate Galectin-1 Deficient Glioma in the Absence of Adaptive Immunity

Gregory J. Baker[1,2], **Peter Chockley**[1,2], **Viveka Nand Yadav**[1,2], **Robert Doherty**[1,2], **Michael Ritt**[2], **Sivaraj Sivaramakrishnan**[2,3], **Maria G. Castro**[1,2], and **Pedro R. Lowenstein**[1,2,*]

[1]Department of Neurosurgery, University of Michigan Medical School, Ann Arbor, MI 48109, USA

[2]Department of Cell and Developmental Biology, University of Michigan Medical School, Ann Arbor, MI 48109, USA

[3]Department of Biomedical Engineering, University of Michigan, Ann Arbor, MI 48109, USA

Abstract

Natural killer (NK) cells safeguard against early tumor formation by destroying transformed target cells in a process referred to as NK immune surveillance. However, the immune escape mechanisms used by malignant brain tumors to subvert this innate type of immune surveillance remain unclear. Here we show that malignant glioma cells suppress NK immune surveillance by overexpressing the β-galactoside-binding lectin galectin-1. Conversely, galectin-1 deficient glioma cells could be eradicated by host NK cells prior to the initiation of an anti-tumor T-cell response. In vitro experiments demonstrated that galectin-1 deficient GL26-Cit glioma cells are ~3-fold more sensitive to NK-mediated tumor lysis that galectin-1 expressing cells. Our findings suggest that galectin-1 suppression in human glioma could improve patient survival by restoring NK immune surveillance that can eradicate glioma cells.

Keywords

galectin-1 (gal-1); natural killer (NK) cells; gal-1 deficient glioma

Introduction

Natural killer (NK) cells represent the main effector lymphocytes of the innate immune system (1, 2). These cells guard against early tumor formation by eliminating transformed cells through NK immune surveillance. NK cells interpret signals on tumor (or virally infected) cells, such as reduced major histocompatibility complex I (MHC-I) expression, as a sign of non-self and/or malignant transformation and lyse such cells when in the context of

*To whom correspondence should be addressed: P.R. Lowenstein, MD, PhD, Richard Schneider Collegiate Professor, Professor, Dept. of Neurosurgery, Professor, Dept. of Cell and Developmental Biology, MSRB II, Room 4570, University of Michigan School of Medicine, 1150 West Medical Center Drive, Ann Arbor, MI 48109-5689 USA, Phone (office) 734-764-0851, pedrol@umich.edu.

Author contributions: G.J.B., M.G.C. and P.R.L. designed research; G.J.B., P.C., V.N.Y. and R.D. performed research; M.R. and S.S. contributed reagents and provided analytical tools; G.J.B., P.C., V.N.Y., M.G.C. and P.R.L. analyzed data; G.J.B., M.G.C. and P.R.L. wrote the paper.

The authors declare no conflicts of interest.

certain co-stimulatory molecules (3, 4). The mechanisms used by malignant brain tumors, such as glioblastoma (GBM), to escape NK-mediated immune surveillance remain poorly understood.

Galectin-1 (gal-1) is a member of a family of β-galactoside-binding lectins. Increased gal-1 expression is detected in primary human prostate, colorectal, bladder, pancreatic, liver, thyroid, ovarian, uterine, cervical, and brain cancers, where its expression is correlated with worse histological grade and poor patient prognosis (5–14). Since it was first shown that cell surface gal-1 induces apoptosis in cytotoxic T-cells (15), it has been proposed that this represents the sole mechanism by which tumor-derived gal-1 suppresses anti-tumor immunity (16–21).

Here we report that shRNA-mediated gal-1 knockdown in glioma cells leads to the rapid accumulation of cytotoxic NK cells within the brain tumor microenvironment that culminates in complete tumor eradication in the absence of an anti-tumor T-cell response. The suppression of glioma-derived gal-1 is predicted to translate into novel therapies for human malignant gliomas by heightening innate anti-tumor NK immune surveillance.

Materials and Methods

Animal strains

Six to seven week-old female C57BL/6J, B6.129S7-*Rag1*^{tm1Mom}/J (i.e RAG1$^{-/-}$), and NOD.Cg-*Prkdc*^{scid} *Il2rg*^{tm1Wjl}/SzJ (i.e. NOD-*scid* IL2Rg^{null} or NSG) mice were purchased from Jackson Laboratory. LEW/SsNHsd Lewis rats (200–240g) were purchased from Harlan Laboratories. All animal experiments were conducted in accordance with procedures approved by the University Committee on Use and Care of Animals (UCUCA) and conformed to the policies and procedures of the Unit for Laboratory Animal Medicine (ULAM) at the University of Michigan.

Cell-lines and Culture Conditions

GL26-Cit, CNS-1-Cit, GL26-Cit-NT, GL26-Cit-EV, CNS-1-Cit-NT, GL26-Cit-gal1i, CNS-1-Cit-gal1i were cultured *in-vitro* under humidified conditions in 95% air/5% CO_2 at 37°C. Culture medium for mCitrine$^+$ glioma cell-lines consisted of Dulbecco's Modified Eagle Medium (DMEM) supplemented with 10% heat-inactivated fetal bovine serum (FBS), 0.3mg/ml L-glutamine, 50U/ml penicillin, 50μg/ml streptomycin, and 6μg/ml G418 selection antibiotic (for selection of the mCitrine expression vector) and were passaged every 2–4 days. In addition to the above reagents, GL26-Cit-NT, GL26-Cit-EV, CNS-1-Cit-NT, GL26-Cit-gal1i, and CNS-1-Cit-gal1i cells were also cultured in the presence of 3μg/ml of puromycin selection antibiotic to select for shRNA expression vectors.

Engineering GL26-Cit, CNS-1-Cit and their respective gal-1 deficient and control shRNA cell-lines

The plasmid containing the mCitrine transgene (pRSET-B-Citrine) was subcloned into the pCI-neo expression vector backbone to afford a 6,199 base-pair plasmid to constitutively express mCitrine fluorescent protein (pCI-neo-mCitrine) (Supplemental Fig. S1). This

plasmid was then used to transfect both wild-type GL26 and CNS-1 cells. Transfected cells were sorted for high mCitrine expression by FACS and cultured under G418 selection antibiotic to maintain transgene expression.

To establish the GL26-Cit-gal1i and CNS-1-Cit-gal1i cell-lines, several pLKO.1-puro lentiviral plasmids encoding both a puromycin resistance cassette and an shRNA hairpin construct specific for rodent galectin-1 (*mlgals1*, NM_008495) mRNA were purchased from Sigma Aldrich as part of the RNAi Consortium. Each shRNA clone was tested for its ability to knockdown gal-1 expression. To do so, a rodent galectin-1 overexpression vector pCMV6-kan/neo-mlgals1 (Origene, Cat#: MC200092) was co-transfected into HEK293 cells along with each of the aforementioned shRNA constructs. RNAi Consortium clone TRCN0000011866 afforded the highest level of gal-1 knockdown and was used to create a second-generation lentiviral vector encoding this *mlgals1*-specfic shRNA (LV-*mLgals1*-11866i). GL26-Cit and CNS-1-Cit cells where then transduced with 80μl of purified LV-*mLgals1*-11866i for 48–72hrs. Infected cells were continually grown under puromycin selection to enrich for transduced cells. Similar methodology was used to create the GL26-Cit-NT, GL26-Cit-EV, and CNS-1-Cit-NT control cell-lines, which also contain the pLKO.1-puro lentiviral expression vector, but either express a non-targeting shRNA hairpin construct (Mission shRNA, Cat#:SHC002, Sigma-Aldrich) or no shRNA insert (empty expression vector) (Mission shRNA, Cat#:SHC001, Sigma-Aldrich).

Primary antibodies used for immunohistochemistry and SDS/PAGE western blot

Purified goat polyclonal anti-mouse galectin-1, (5μg/ml), Cat#: AF1245, R&D Systems; purified rabbit polyclonal anti-cleaved caspase-3 (Asp 175), (1:300), Cat#:9661, Cell Signaling; purified hamster anti-mouse CD49b (DX5), (1:500), Cat#:103507, Biolegend; purified rat anti-mouse NKp46 (29A1.4), (1:500), Cat#:560754, BD Pharmigen; FITC-conjugated mouse anti-granzyme B (GB11), (1:1,000), Cat#:515403, Biolegend; purified Armenian hamster anti-mouse CD3 ε (145-2C11), (1:500), Cat#: 553057, BD Pharmingen. Note: no surfactants or antigen retrieval steps were used in any NK cell or T-cell immunolabeling procedure. Detailed immunohistochemical and SDS/PAGE Western blot methodology can be found in the Supplemental Experimental Procedures section available online.

Stereotactic tumor implantation and processing of tissue samples

We have previously described the procedure for stereotactic intracranial tumor implantation into the rodent brain (22). A brief description of the stereotactic tumor implantation and transcardial perfusion procedures can be found in the Supplemental Experimental Procedures section available online.

In-vivo immunodepletion studies

The following antibodies were administered intraperitoneally to deplete NK cells (or basophils) (per mouse): 25μL of stock rabbit polyclonal anti-asialo GM_1, Cat#: 986-10001, Wako, diluted to a final volume of 100μL in ddH_2O administered one day before and after tumor implantation, then every three days; 100μL of undiluted normal rabbit serum, Cat#: 16120, Life Technologies, administered one day before and after tumor implantation then

every three days; 200μg of mouse monoclonal anti-NK1.1 functional grade purified (clone:PK136), Cat#: 16-5941, eBioscience diluted to a final volume of 400μL in sterile Dulbecco's phosphate buffered saline (DPBS) pH7.4 and administered two days prior to tumor implantation and every four days; 400μL (equivalent to 200μg) of undiluted purified mouse IgG2a, kappa isotype control antibody (clone:MG2a-53), Cat#: 401502, BioLegend, administered two days prior to tumor implantation and every four days; 300μL (equivalent to 30μg) of undiluted rat monoclonal anti-CD200R3 (clone:ba103), Cat#: HM1103, Hycult biotech, administered one day prior to tumor implantation and every 5 days; 30μL (equivalent to 30μg) of purified rat IgG2b, kappa isotype control antibody (clone:RTK4530), Cat#: 400637, BioLegend, diluted to a final volume of 300μL in 0.9%NaCl administered one day prior to tumor implantation and every 5 days.

Antibodies used for flow cytometry

NK cells were isolated using mouse monoclonal APC-conjugated NK1.1 (PK136), Cat#: 17-5941-82, eBioscience; and Syrian hamster pacific blue-conjugated CD3 ε (500A2), Cat#: 558214, BD Pharmingen. Glioma-infiltrating NK cells were analyzed using PE-conjugated rat anti-mouse CD45 (3OF11), Cat#:553081, BD Pharmigen; APC-conjugated mouse anti-mouse NK1.1 (PK136), Cat#:17-5941-82, eBioscience; Pacific blue-conjugated syrian hamster CD3 ε (500A2), Cat#: 558214, BD Pharmingen; and FITC-conjugated mouse monoclonal anti-granzyme B (GB11), Cat#:515403, Biolegend. Details on the harvesting and processing of whole splenocytes and glioma-infiltrating lymphocytes can be found in the Supplemental Experimental Procedures section available online and at the following reference (23).

ELISpot

Details on the ELISpot procedure can be found in the Supplemental Experimental Procedures section available online.

Fluorimetry

Details on the fluorimetry procedure can be found in the Supplemental Experimental Procedures section available online.

Statistical analysis

Statistical analyses were performed using GraphPad Prism5 (GraphPad Software, Inc.). Data are reported as mean ± SEM and were examined with the statistical tests specified in each figure legend. Values were considered significant at the $p \leq 0.05$ level.

Accession numbers

Mouse GL26 brain tumor microarray data are available at the NCBI Gene Expression Omnibus (GEO) database (http://www.ncbi.nlm.nih.gov/geo/), accession number GSE11420.

Results

Gal-1 knockdown in mouse GL26-Cit glioma cells causes an *in-vivo*-specific growth deficiency

Examination of genome-wide microarray data from mouse GL26 gliomas harvested from the brains of syngeneic C57BL/6 mice (NCBI GEO database, accession GSE11420) revealed that gal-1 (*mLgals1*) was the most abundantly expressed mRNA transcript in mouse GL26 glioma. We became interested in testing the role of this gene in brain tumor growth and invasion because tumor-derived gal-1 is associated with increasing malignancy and poor patient prognosis in clinical glioma (Supplemental Fig. S2) (13, 14).

We began by determining whether gal-1 was also expressed by a fluorescently-modified version of GL26 referred to as GL26-Cit. Western blot and immunohistochemistry confirmed the expression of gal-1 by GL26-Cit cells (Fig. 1A and B). We validated 5 commercially available gal-1-specific shRNA hairpins from the RNAi Consortium (TRC) and chose the one that exhibited the highest degree of gal-1 knockdown for stable incorporation into GL26-Cit cells by lentiviral-mediated gene transfer. Resultant gal-1 deficient cells were referred to as GL26-Cit-gal1i. These cells exhibited a 60% reduction in gal-1 protein expression relative to control GL26-Cit cells transduced with lentiviruses expressing a non-targeting shRNA (GL26-Cit-NT) or an empty shRNA expression vector (GL26-Cit-EV) (Fig. 1A, C and S3A). Two independent transductions of either gal-1-specific-, or control-, shRNA hairpins were performed (Supplemental Fig. S3).

To characterize the growth and behavior of GL26-Cit-gal1i *in-vitro*, we first performed ELISA analysis for secreted gal-1 which revealed that GL26-Cit-gal1i cells release half as much gal-1 into cell culture media compared to equivalent numbers of GL26-Cit-NT (Fig. 1D). We also determined the average cell doubling-time of GL26-Cit-gal1i cells compared to GL26-Cit-NT over a 96hr growth period starting from an initial seeding density of 4.8×10^2 cells per cm^2. Both cell-lines displayed cell doubling-times of approximately 16hrs (Fig. 1E) with no significant differences in the rate of spontaneous apoptosis (Supplemental Fig. S4). *In-vitro* scratch assays were performed to evaluate the migration speed of GL26-Cit-gal1i cells compared to GL26-Cit-NT. GL26-Cit-gal1i cells exhibited a nearly 25% increase in migration distance compared to GL26-Cit-NT when cultured on fibronectin, a binding partner for heterotypic gal-1 interaction (Fig. 1F) (24).

To assess GL26-Cit-gal1i growth *in-vivo*, we implanted 3×10^4 cells into the striatum of $RAG1^{-/-}$ mice (25) and compared their invasion characteristics to control GL26-Cit, GL26-Cit-EV and GL26-Cit-NT cells after 48hrs. We used $RAG1^{-/-}$ mice, which do not produce mature T- and B-cells, to avoid antigen-specific adaptive immunity against mCitrine fluorescent protein so not to obscure our analysis of tumor invasion. Tumor morphology was analyzed by fluorescence confocal microscopy of tumor-derived mCitrine. Control GL26-Cit cell-lines expressing normal gal-1 levels displayed a diffuse growth pattern indicative of perivascular tumor invasion, while GL26-Cit-gal1i cells remained confined to the site of initial tumor implantation (Fig. 1G). This effect was quantified by comparing the morphologies of GL26-Cit-gal1i gliomas with controls using ImageJ analytical software (Supplementary Fig. S5).

Gal-1 deficient glioma cells undergo early caspase-3-dependent cell-death upon implantation into the RAG1$^{-/-}$ mouse brain

Encouraged by our observation that GL26-Cit-gal1i glioma cells fail to invade the mouse brain, we wished to test whether gal-1 suppression would improve the median survival of mice bearing GL26-Cit glioma. Kaplan-Meier survival analysis was carried out on RAG1$^{-/-}$ mice implanted with 3×10^4 GL26-Cit-gal1i, GL26-Cit or GL26-Cit-NT glioma cells to compare their survival rates (Fig. 2A). All mice in the GL26-Cit and GL26-Cit-NT groups became moribund by day 20 post-tumor implantation, yet each mouse implanted with GL26-Cit-gal1i cells survived 100 days post-tumor implantation (dpi). Mice implanted with GL26-Cit-gal1i cells were then electively euthanized to assess tumor burden. While GL26-Cit and GL26-Cit-NT cells formed tumors comprising most of the ipsilateral striatum after 20 days *in-vivo*, only non-viable remnants of mCitrine were found in the brain of mice implanted with GL26-Cit-gal1i cells after the 100th day *in-vivo* (Fig. 2B).

To characterize the fate of intracranially implanted GL26-Cit-gal1i cells, we analyzed tumors corresponding to 7 time-points over a 9-day growth period (n=21; 3 mice/time-point). Fluorescence immunohistochemistry for cleaved caspase-3, a major downstream effector caspase mediating apoptotic cell-death (26), revealed large numbers of GL26-Cit-gal1i cells undergoing apoptotic cell-death, especially at the invasive tumor margin, within 3-days of tumor implantation (Fig. 2C). Later tumors exhibited exacerbated lysis culminating in complete tumor lysis after 9-days *in-vivo* (Fig. 2D). Interestingly, antibodies against cleaved caspase -8 and -9, initiator caspases of the extrinsic and intrinsic caspase cascades, respectively, failed to detect activated upstream caspases (data not shown), suggesting that pro-capase-3 was being cleaved directly.

We considered that the innate immune system might play a role in the regression of GL26-Cit-gal1i glioma in the RAG1$^{-/-}$ model. To test this hypothesis, we implanted GL26-Cit-gal1i cells into the striatum of NOD-*scid* IL2Rg^{null} (i.e. NSG) mice, a mouse strain lacking both innate and adaptive immunity (27), for comparison with GL26-Cit-NT cells (n=6; 3 mice/group). We reasoned that if the RAG1$^{-/-}$ innate immune system was responsible for GL26-Cit-gal1i regression, then GL26-Cit-gal1i tumor growth should be restored on implantation into NSG mice. Our hypothesis was substantiated, as 3×10^4 GL26-Cit-gal1i or GL26-Cit-NT cells both formed lethal brain tumors in NSG mice after 16-days *in-vivo* (Fig. 2E). The combined results of GL26-Cit-gal1i rejection in RAG1$^{-/-}$ mice, and the restoration of lethal tumor growth in NSG mice, strongly implicated the innate immune response in the acute rejection of intracranial GL26-Cit-gal1i glioma.

NK cells mediate the acute rejection of intracranial gal-1 deficient glioma

NK cells lyse tumor target cells through the release of granzyme B (GzmB), an enzyme that directly cleaves pro-caspase-3 (28–30). Because our data had shown that GL26-Cit-gal1i tumors were positive for cleaved caspase-3, yet negative for activated upstream initiator caspases -8 and -9, we questioned whether NK cells are responsible for GL26-Cit-gal1i rejection in RAG1$^{-/-}$ mice. We therefore treated RAG1$^{-/-}$ mice bearing GL26-Cit-gal1i glioma with anti-asialo GM_1, an antiserum validated by ourselves (Supplementary Fig. S6A and B), and others (31), to deplete NK cells in mice, or with normal rabbit serum as a

negative control. Mice were euthanized 16dpi and their brains were imaged using epifluorescence microscopy. Treatment with anti-asialo GM_1 caused the formation of large intracranial GL26-Cit-gal1i tumors, while treatment with normal rabbit serum control failed to do so (Fig. 3A).

We tested whether the growth of GL26-Cit-gal1i glioma permitted by anti-asialo GM_1 was mediated by off-target depletion of basophils as previously described (32). Cohorts of $RAG1^{-/-}$ mice was treated with anti-CD200R3 (clone: Ba103), a monoclonal antibody validated for *in-vivo* depletion of basophils (33) or rat IgG2b isotype control antibodies at an equivalent dose, route, and schedule. Both anti-CD200R3 and rat IgG2b isotype control antibodies failed to permit intracranial GL26-Cit-gal1i tumor growth in $RAG1^{-/-}$ mice after a 10-day growth period (Supplementary Fig. S6C), indicating that basophils are not responsible for gal-1 deficient glioma rejection in $RAG1^{-/-}$ mice.

We confirmed our results with anti-asialo GM_1 using purified functional-grade anti-NK1.1 (clone: PK136) (34), an alternative monoclonal antibody validated for *in-vivo* NK depletion in C57BL/6 mice. $RAG1^{-/-}$ mice treated with anti-NK1.1 also formed large GL26-Cit-gal1i tumors of equivalent size to those obtained with anti-asialo GM_1 (Fig. 3B).

Gal-1 deficient gliomas are more heavily infiltrated with granzyme B^+ NK cells

We next sought to evaluate the presence of glioma-infiltrating NK cells. We implanted 3×10^4 GL26-Cit-gal1i or GL26-Cit-NT cells into the striatum of $RAG1^{-/-}$ mice and allowed for 5-days of tumor growth (n=6; 3 mice/group). Mouse brains were harvested, sectioned and immunolabeled with GzmB-specific antibodies. Quantitative analysis revealed that GL26-Cit-gal1i tumors contain nearly 8 times more GzmB compared to GL26-Cit-NT (Fig. 4A–C).

Because $RAG1^{-/-}$ mice do not produce mature T-lymphocytes, the GzmB signal seen in GL26-Cit-gal1i tumors was reasoned to be NK-specific. To confirm this, we performed multi-color flow cytometric analysis on glioma-infiltrating NK cells using antibodies against CD45, NK1.1, CD3 ε, GzmB, and IFN-γ after 5-days of *in-vivo* growth in the $RAG1^{-/-}$ mouse brain. GL26-Cit-gal1i tumors contained significantly higher percentages of $GzmB^+$ NK cells compared to GL26-Cit-NT (48.67 ± 5.87% gal1i vs. 22.30 ± 6.60% NT) (Fig. 4D), while GL26-Cit-NT gliomas contained significantly higher percentages of IFN-γ^+ NK cells (36.12 ± 6.62% NT vs. 12.29 ± 1.08% gal1i) (Fig. 4E). Further confirmation of tumor-infiltrating NK cells was obtained through immunohistochemistry with alternative NK-specific antibodies CD49b/DX5 (Fig. 4F) and NKp46 (Fig. 4G), which indicate that NK cells are capable of infiltrating both NT and gal1i gliomas.

NK cells eradicate gal-1 deficient glioma prior to the initiation of an adaptive immune response

We next investigated the effect of NK cells on the rejection of gal-1 deficient glioma in fully immunocompetent hosts. We implanted 3×10^4 GL26-Cit-gal1i or GL26-Cit-NT cells into the striatum of wild-type C57BL/6J mice and treated these mice with anti-asialo GM_1 or control serum for 5-days prior to sacrifice (n=12; 3 mice/group/treatment). Restriction of our

analysis to the first 5dpi allowed us to isolate the innate immune response, as antigen-specific adaptive immunity does not peak until ~10–14dpi (35–39). Mice implanted with GL26-Cit-NT cells formed equivalently sized tumors after 5-days of growth regardless of treatment with anti-asialo GM_1 or control serum (Fig. 5A). However, mice implanted with GL26-Cit-gal1i only formed tumors similar in size to GL26-Cit-NT when treated with NK-depleting anti-asialo GM_1 (Fig. 5B). We quantified this effect by calculating the average tumor area in each treatment group using ImageJ analytical software (Fig. 5C). GL26-Cit-gal1i tumors treated with control serum were significantly smaller than those in the three other treatment groups. This result shows that the NK cells from fully immunocompetent hosts are capable of efficiently eradicating gal-1 deficient glioma.

We then asked whether the innate immune system could effectively eliminate GL26-Cit-gal1i glioma prior to the initiation of an antigen-specific adaptive immune response. To address this, we implanted 3×10^4 GL26-Cit-gal1i cells into the striatum of wild-type C57BL/6J mice, and treated mice with either anti-asialo GM_1 or control serum for 16-days prior to sacrifice to provide enough time for the onset of antigen-specific adaptive immunity. The brain and spleen of each mouse were freshly harvested at the time of sacrifice and a fraction of total splenocytes from each mouse was immunolabeled with anti-NK1.1 and anti-CD3 ε antibodies to assess NK cell depletion by flow cytometric analysis. Mice treated with anti-asialo GM_1 exhibited a >4-fold reduction in the average percentage of splenic-derived NK cells (Fig. 5D and F) without altering the average percentage of T-cells (Fig. 5E and G).

The remaining splenocytes were used in antigen-induced ELISpot analysis to evaluate the number of splenocytes secreting IFN-γ in response to GL26-Cit-gal1i lysate after 48hrs *in-vitro*. This assay served as a surrogate indicator of the degree of adaptive immune activation elicited against GL26-Cit-gal1i brain tumors over the 16-day growth period. ELISpot results revealed that more splenocytes from mice treated with anti-asialo GM_1 secreted IFN-γ in response to addition of GL26-Cit-gal1i lysate compared to those treated with normal rabbit serum (Fig. 5H). This suggested that GL26-Cit-gal1i tumors were present in the brain long enough to be recognized by the adaptive immune response in mice depleted of NK cells. However, the paucity of splenocytes secreting IFN-γ in response to GL26-Cit-gal1i lysate from mice treated with control serum indicated that NK cells eradicate GL26-Cit-gal1i tumors prior to recognition by antigen-specific anti-tumor immunity. Analysis of corresponding brain tumor size confirmed this notion by showing that gliomas were present in the brains of mice treated with anti-asialo GM_1, while no tumors were seen in the brains of mice treated with normal rabbit serum (Fig. 5I). We observed a strong inverse Pearson's product-moment correlation coefficient ($r = -0.91$) between the average number of IFN-γ spots from our ELISpot analysis and the corresponding tumor size in mice treated with anti-asialo GM_1. We conclude that reductions in brain tumor burden in mice lacking NK cells correlates with the magnitude of antigen-specific adaptive immunity. Immunohistochemistry with anti-CD3 ε antibodies revealed that only the mice treated with anti-asialo GM_1 contained brain-infiltrating T-cells (Supplemental Fig. S7).

Gal-1 deficient rat CNS-1-Cit glioma cells fail to grow intracranially

We have asked whether gal-1 deficient glioma of other species fail to grow intracranially. For this, we validated gal-1 expression in fluorescently-modified rat CNS-1 glioma cells also expressing mCitrine fluorescent protein, referred to as CNS-1-Cit. Gal-1 expression was silenced through stable incorporation of gal-1-specific shRNA by lentiviral-mediated gene transfer to generate CNS-1-Cit-gal1i. CNS-1-Cit-gal1i cells exhibited a 50% reduction in gal-1 protein expression relative to control CNS-1-Cit cells infected with lentiviruses expressing a non-targeting shRNA referred to as CNS-1-Cit-NT (Fig. 6A). We implanted 3×10^4 CNS-1-Cit-gal1i or CNS-1-Cit-NT cells into the striatum of syngeneic Lewis rats and electively euthanized after 8dpi to preclude the onset of an adaptive anti-tumor immune response. While CNS-1-Cit-NT cells formed viable tumors in each rat brain after the 8-day growth period, CNS-1-Cit-gal1i tumors were completely rejected, leaving remnants of mCitrine at the site of initial tumor implantation (Fig. 6B). We conclude that gal-1 suppression sensitizes glioma of diverse species to innate immune attack.

Gal-1 deficient glioma cells are sensitized to NK-mediated cytotoxicity *in-vitro*

We next examined the efficiency of NK-mediated gal-1 deficient tumor lysis *in-vitro*. Splenic-derived NK cells were isolated from tumor-naïve RAG1 $^{-/-}$ mice by FACS and determined to be >95% pure (Supplementary Fig. S8). NK cells were pre-stimulated overnight in round-bottom wells with 8 concentrations of interleukin-12 (IL-12) and interleukin-15 (IL-15) from 0–10,000 pg/ml of each cytokine. Stimulated NK cells were added to both GL26-Cit-gal1i and GL26-Cit-NT glioma cells at an effector-to-target (E:T) ratio of 20:1 and incubated for 4hrs at 37°C/5%CO_2. While unstimulated NK cells failed to induce lysis in either glioma cell-line, GL26-Cit-gal1i cells lysed more readily after the 4hr co-incubation with NK cells stimulated with IL-12/15 concentrations above 312.5pg/ml (Fig. 7A). Linear regression analysis comparing IL-12/15 concentration with the resultant percentage of $GzmB^+$ NK cells after overnight stimulation revealed an R-squared value of 0.94 (R^2=0.94), demonstrating that IL-12/15 stimulation strongly correlates with GzmB production by splenic-derived NK cells (Fig. 7B).

Linear regression analysis also revealed a positive correlation between the percentage of $GzmB^+$ NK cells and the percentage of tumor lysis in the Gl26-Cit-gal1i group (R^2=0.92), which were less correlated in the GL26-Cit-NT group (R^2=0.74) (Fig. 7C). We interpret this result as an indicator of NK cytotoxic potential; how other NK proteins relate to tumor NK cytotoxicity remains to be determined (40, 41). The reduced correlation between GzmB expression and tumor lysis in the GL26-Cit-NT group suggested that gal-1 expression imparts glioma cells with intrinsic resistance to NK-mediated tumor lysis. A sigmoidal dose-response fitting of log-transformed IL-12/15 concentration versus percentage tumor lysis revealed corresponding EC_{50} values for IL-12/15 stimulation (i.e. amount of IL-12/15 required to elicit 50% tumor cell lysis) of 2,985pg/ml and 10,592pg/ml for Gl26-Cit-gal1i and GL26-Cit-NT cells, respectively. This result demonstrates that GL26-Cit-gal1i cells are 3.55-fold more sensitive to NK-mediated cytotoxicity compared to GL26-Cit-NT *in-vitro* (Fig. 7D).

To test whether gal-1 directly inhibits NK cell function or viability, we added recombinant mouse gal-1 protein at increasing concentrations to NK/GL26-Cit-gal1i *in-vitro* co-cultures. Unstimulated splenic-derived NK cells failed to induce tumor cell lysis, while those stimulated with 10,000pg/ml IL-12/15 induced tumor cell death after 4hr co-incubation. However, application of increasing levels of recombinant gal-1 protein failed to inhibit NK-mediated cytotoxicity (Fig. 7E) or induce apoptosis in either unstimulated or stimulated NK cells (Fig. 7F).

Discussion

We have identified glioma-derived galectin-1 as a potent suppressor of anti-tumor NK immune surveillance. Five *in-vivo* experimental results support this conclusion: (i.) gal-1 deficient glioma cells fail to form lethal brain tumors upon orthotopic implantation into the $RAG1^{-/-}$ mouse brain; (ii.) lethal gal-1 deficient glioma growth is restored upon implantation into the brains of NOD-*scid* $IL2Rg^{null}$ mice; (iii.) immunodepletion of NK cells with anti-asialo GM_1 anti-serum or anti-NK1.1 monoclonal antibodies permit the formation of lethal gal-1 deficient gliomas in $RAG1^{-/-}$ mice; (iv.) gal-1 deficient gliomas in $RAG1^{-/-}$ mice contain more $GzmB^{+}$ NK cells; and (v.) NK cells eradicate gal-1 deficient gliomas in fully immunocompetent C57BL/6J mice prior to the initiation of anti-tumor T-cell responses.

Flow cytometric and immunohistochemical data on tumor-infiltrating NK cells demonstrate the accumulation of $GzmB^{+}$ NK cells specifically within gal-1 deficient gliomas soon after implantation. However, gliomas expressing normal levels of gal-1 are infiltrated with NK cells that predominantly produce IFN-γ instead of GzmB.

Experiments in fully immunocompetent C57BL/6J mice demonstrated that the innate immune system rejects gal-1 deficient glioma without the support of antigen-specific anti-tumor adaptive immunity. This is shown by the absence of growing brain tumors and anti-tumor T-cell responses in mice treated with control antiserum. As expected, in the absence of NK cells, gal-1 deficient gliomas are targets of tumor-specific cytotoxic T-cells, albeit later in tumor progression. This is evidenced by the negative correlation between the levels of antigen-specific T-cell responses and brain tumor size in immunocompetent mice depleted of NK cells.

Glioma cells evade cytotoxic T-cell recognition and lysis by downregulating MHC classI proteins (42, 43). However, this process increases their sensitivity to NK-mediated attack, as cells with reduced expression of MHC class-I proteins are targets of NK immune surveillance (42). Upregulation of gal-1 expression may therefore provide an advantage for glioma cells to concurrently curb both arms of the anti-tumor immune response by counteracting the increased sensitivity to NK immune surveillance associated with MHC-1 downregulation.

Our results introduce a paradigm shift in the current understanding of anti-glioma immune-mediated control by showing for the first time that NK cells, even in the absence of adaptive immunity, eradicate intracranial glioma in the context of reduced tumor-derived gal-1. We

predict that gal-1 suppression; either alone, or in combination with other immunotherapeutic strategies (i.e. dendritic cell vaccination (44, 45) and/or gene therapy (46–49) will provide dramatic clinical improvements in patients suffering from malignant brain tumors.

Supplementary Material

Refer to Web version on PubMed Central for supplementary material.

Acknowledgments

This work was supported by National Institutes of Health/National Institute of Neurological Disorders & Stroke (NIH/NINDS) grants 1RO1-NS 054193, 1RO1-NS 061107, and 1RO1-NS082311 to P.R.L.; and grants 1UO1-NS052465, 1RO1-NS 057711, and 1RO1-NS074387 to M.G.C. We gratefully acknowledge support for our work received from Mr. Philip Jenkins, and the Department of Neurosurgery, University of Michigan School of Medicine. We are also grateful to Dr. Karin Muraszko for her academic leadership, Molly Dahlgren, D. Tomford, and S. Napolitan for their superb administrative support, and to Dr. Roger Tsien (UCSD) for kindly donating the pRSET-B-mCitrine plasmid.

References

1. Vivier E, Raulet DH, Moretta A, Caligiuri MA, Zitvogel L, Lanier LL, et al. Innate or adaptive immunity? The example of natural killer cells. Science. 2011; 331:44–9. [PubMed: 21212348]
2. Vivier E, Tomasello E, Baratin M, Walzer T, Ugolini S. Functions of natural killer cells. Nat Immunol. 2008; 9:503–10. [PubMed: 18425107]
3. Bryceson YT, March ME, Ljunggren HG, Long EO. Activation, coactivation, and costimulation of resting human natural killer cells. Immunol Rev. 2006; 214:73–91. [PubMed: 17100877]
4. Smyth MJ, Hayakawa Y, Takeda K, Yagita H. New aspects of natural-killer-cell surveillance and therapy of cancer. Nat Rev Cancer. 2002; 2:850–61. [PubMed: 12415255]
5. Wu H, Chen P, Liao R, Li YW, Yi Y, Wang JX, et al. Overexpression of galectin-1 is associated with poor prognosis in human hepatocellular carcinoma following resection. J Gastroenterol Hepatol. 2012; 27:1312–9. [PubMed: 22432916]
6. Kim HJ, Jeon HK, Cho YJ, Park YA, Choi JJ, Do IG, et al. High galectin-1 expression correlates with poor prognosis and is involved in epithelial ovarian cancer proliferation and invasion. Eur J Cancer. 2012; 48:1914–21. [PubMed: 22386573]
7. van den Brule FA, Waltregny D, Castronovo V. Increased expression of galectin-1 in carcinoma-associated stroma predicts poor outcome in prostate carcinoma patients. J Pathol. 2001; 193:80–7. [PubMed: 11169519]
8. Kohrenhagen N, Volker HU, Kapp M, Dietl J, Kammerer U. Increased expression of galectin-1 during the progression of cervical neoplasia. Int J Gynecol Cancer. 2006; 16:2018–22. [PubMed: 17177840]
9. Sanjuan X, Fernandez PL, Castells A, Castronovo V, van den Brule F, Liu FT, et al. Differential expression of galectin 3 and galectin 1 in colorectal cancer progression. Gastroenterology. 1997; 113:1906–15. [PubMed: 9394730]
10. Berberat PO, Friess H, Wang L, Zhu Z, Bley T, Frigeri L, et al. Comparative analysis of galectins in primary tumors and tumor metastasis in human pancreatic cancer. JHistochem Cytochem. 2001; 49:539–49. [PubMed: 11259457]
11. Chiariotti L, Berlingieri MT, Battaglia C, Benvenuto G, Martelli ML, Salvatore P, et al. Expression of galectin-1 in normal human thyroid gland and in differentiated and poorly differentiated thyroid tumors. Int J Cancer. 1995; 64:171–5. [PubMed: 7622305]
12. van den Brule FA, Buicu C, Berchuck A, Bast RC, Deprez M, Liu FT, et al. Expression of the 67-kD laminin receptor, galectin-1, and galectin-3 in advanced human uterine adenocarcinoma. Hum Pathol. 1996; 27:1185–91. [PubMed: 8912829]
13. Camby I, Belot N, Rorive S, Lefranc F, Maurage CA, Lahm H, et al. Galectins are differentially expressed in supratentorial pilocytic astrocytomas, astrocytomas, anaplastic astrocytomas and

glioblastomas, and significantly modulate tumor astrocyte migration. Brain Pathol. 2001; 11:12–26. [PubMed: 11145198]

14. Rorive S, Belot N, Decaestecker C, Lefranc F, Gordower L, Micik S, et al. Galectin-1 is highly expressed in human gliomas with relevance for modulation of invasion of tumor astrocytes into the brain parenchyma. Glia. 2001; 33:241–55. [PubMed: 11241742]
15. Perillo NL, Pace KE, Seilhamer JJ, Baum LG. Apoptosis of T cells mediated by galectin-1. Nature. 1995; 378:736–9. [PubMed: 7501023]
16. Rubinstein N, Alvarez M, Zwirner NW, Toscano MA, Ilarregui JM, Bravo A, et al. Targeted inhibition of galectin-1 gene expression in tumor cells results in heightened T cell-mediated rejection; A potential mechanism of tumor-immune privilege. Cancer Cell. 2004; 5:241–51. [PubMed: 15050916]
17. Gieseke F, Bohringer J, Bussolari R, Dominici M, Handgretinger R, Muller I. Human multipotent mesenchymal stromal cells use galectin-1 to inhibit immune effector cells. Blood. 2010; 116:3770–9. [PubMed: 20644118]
18. Banh A, Zhang J, Cao H, Bouley DM, Kwok S, Kong C, et al. Tumor galectin-1 mediates tumor growth and metastasis through regulation of T-cell apoptosis. Cancer Res. 2011; 71:4423–31. [PubMed: 21546572]
19. Soldati R, Berger E, Zenclussen AC, Jorch G, Lode HN, Salatino M, et al. Neuroblastoma triggers an immunoevasive program involving galectin-1-dependent modulation of T cell and dendritic cell compartments. Int J Cancer. 2012; 131:1131–41. [PubMed: 22020795]
20. Kovacs-Solyom F, Blasko A, Fajka-Boja R, Katona RL, Vegh L, Novak J, et al. Mechanism of tumor cell-induced T-cell apoptosis mediated by galectin-1. Immunol Lett. 2010; 127:108–18. [PubMed: 19874850]
21. Cedeno-Laurent F, Watanabe R, Teague JE, Kupper TS, Clark RA, Dimitroff CJ. Galectin-1 inhibits the viability, proliferation, and Th1 cytokine production of nonmalignant T cells in patients with leukemic cutaneous T-cell lymphoma. Blood. 2012; 119:3534–8. [PubMed: 22383798]
22. Puntel M, Kroeger KM, Sanderson NS, Thomas CE, Castro MG, Lowenstein PR. Gene transfer into rat brain using adenoviral vectors. Curr Protoc Neurosci. 2010; Chapter 4(Unit 4):24. [PubMed: 20066657]
23. Curtin JF, Liu N, Candolfi M, Xiong W, Assi H, Yagiz K, et al. HMGB1 mediates endogenous TLR2 activation and brain tumor regression. PLoS Med. 2009; 6:e10. [PubMed: 19143470]
24. Ozeki Y, Matsui T, Yamamoto Y, Funahashi M, Hamako J, Titani K. Tissue fibronectin is an endogenous ligand for galectin-1. Glycobiology. 1995; 5:255–61. [PubMed: 7780201]
25. Mombaerts P, Iacomini J, Johnson RS, Herrup K, Tonegawa S, Papaioannou VE. RAG-1-deficient mice have no mature B and T lymphocytes. Cell. 1992; 68:869–77. [PubMed: 1547488]
26. Tewari M, Quan LT, O'Rourke K, Desnoyers S, Zeng Z, Beidler DR, et al. Yama/CPP32 beta, a mammalian homolog of CED-3, is a CrmA-inhibitable protease that cleaves the death substrate poly(ADP-ribose) polymerase. Cell. 1995; 81:801–9. [PubMed: 7774019]
27. Shultz LD, Lyons BL, Burzenski LM, Gott B, Chen X, Chaleff S, et al. Human lymphoid and myeloid cell development in NOD/LtSz-scid IL2R gamma null mice engrafted with mobilized human hemopoietic stem cells. J Immunol. 2005; 174:6477–89. [PubMed: 15879151]
28. Barry M, Heibein JA, Pinkoski MJ, Lee SF, Moyer RW, Green DR, et al. Granzyme B short-circuits the need for caspase 8 activity during granule-mediated cytotoxic T-lymphocyte killing by directly cleaving Bid. Mol Cell Biol. 2000; 20:3781–94. [PubMed: 10805722]
29. Goping IS, Barry M, Liston P, Sawchuk T, Constantinescu G, Michalak KM, et al. Granzyme B-induced apoptosis requires both direct caspase activation and relief of caspase inhibition. Immunity. 2003; 18:355–65. [PubMed: 12648453]
30. Metkar SS, Wang B, Ebbs ML, Kim JH, Lee YJ, Raja SM, et al. Granzyme B activates procaspase-3 which signals a mitochondrial amplification loop for maximal apoptosis. J Cell Biol. 2003; 160:875–85. [PubMed: 12629051]
31. Kasai M, Yoneda T, Habu S, Maruyama Y, Okumura K, Tokunaga T. In vivo effect of anti-asialo GM1 antibody on natural killer activity. Nature. 1981; 291:334–5. [PubMed: 7231554]

32. Nishikado H, Mukai K, Kawano Y, Minegishi Y, Karasuyama H. NK cell-depleting anti-asialo GM1 antibody exhibits a lethal off-target effect on basophils in vivo. JImmunol. 2011; 186:5766–71. [PubMed: 21490162]
33. Obata K, Mukai K, Tsujimura Y, Ishiwata K, Kawano Y, Minegishi Y, et al. Basophils are essential initiators of a novel type of chronic allergic inflammation. Blood. 2007; 110:913–20. [PubMed: 17409268]
34. Harshan KV, Gangadharam PR. In vivo depletion of natural killer cell activity leads to enhanced multiplication of Mycobacterium avium complex in mice. Infect Immun. 1991; 59:2818–21. [PubMed: 1855997]
35. Zirger JM, Puntel M, Bergeron J, Wibowo M, Moridzadeh R, Bondale N, et al. Immune-mediated loss of transgene expression from virally transduced brain cells is irreversible, mediated by IFNgamma, perforin, and TNFalpha, and due to the elimination of transduced cells. Mol Ther. 2012; 20:808–19. [PubMed: 22233583]
36. Kennedy BC, Maier LM, D'Amico R, Mandigo CE, Fontana EJ, Waziri A, et al. Dynamics of central and peripheral immunomodulation in a murine glioma model. BMC Immunol. 2009; 10:11. [PubMed: 19226468]
37. Kalos M, June CH. Adoptive T cell transfer for cancer immunotherapy in the era of synthetic biology. Immunity. 2013; 39:49–60. [PubMed: 23890063]
38. Gajewski TF, Schreiber H, Fu YX. Innate and adaptive immune cells in the tumor microenvironment. Nat Immunol. 2013; 14:1014–22. [PubMed: 24048123]
39. Wraith DC, Nicholson LB. The adaptive immune system in diseases of the central nervous system. J Clin Invest. 2012; 122:1172–9. [PubMed: 22466659]
40. Alter G, Malenfant JM, Altfeld M. CD107a as a functional marker for the identification of natural killer cell activity. J Immunol Methods. 2004; 294:15–22. [PubMed: 15604012]
41. Russell JH, Ley TJ. Lymphocyte-mediated cytotoxicity. Annu Rev Immunol. 2002; 20:323–70. [PubMed: 11861606]
42. Bubenik J. MHC class I down-regulation: tumour escape from immune surveillance?(review). Int J Oncol. 2004; 25:487–91. [PubMed: 15254748]
43. Zagzag D, Salnikow K, Chiriboga L, Yee H, Lan L, Ali MA, et al. Downregulation of major histocompatibility complex antigens in invading glioma cells: stealth invasion of the brain. Lab Invest. 2005; 85:328–41. [PubMed: 15716863]
44. Kim W, Liau LM. Dendritic cell vaccines for brain tumors. Neurosurg Clin N Am. 2010; 21:139–57. [PubMed: 19944973]
45. Bregy A, Wong TM, Shah AH, Goldberg JM, Komotar RJ. Active immunotherapy using dendritic cells in the treatment of glioblastoma multiforme. Cancer Treat Rev. 2013; 39:891–907. [PubMed: 23790634]
46. Tobias A, Ahmed A, Moon KS, Lesniak MS. The art of gene therapy for glioma: a review of the challenging road to the bedside. J Neurol Neurosurg Psychiatry. 2013; 84:213–22. [PubMed: 22993449]
47. Assi H, Candolfi M, Baker G, Mineharu Y, Lowenstein PR, Castro MG. Gene therapy for brain tumors: basic developments and clinical implementation. Neurosci Lett. 2012; 527:71–7. [PubMed: 22906921]
48. Mohyeldin A, Chiocca EA. Gene and viral therapy for glioblastoma: a review of clinical trials and future directions. Cancer J. 2012; 18:82–8. [PubMed: 22290261]
49. Simonato M, Bennett J, Boulis NM, Castro MG, Fink DJ, Goins WF, et al. Progress in gene therapy for neurological disorders. Nat Rev Neurol. 2013; 9:277–91. [PubMed: 23609618]

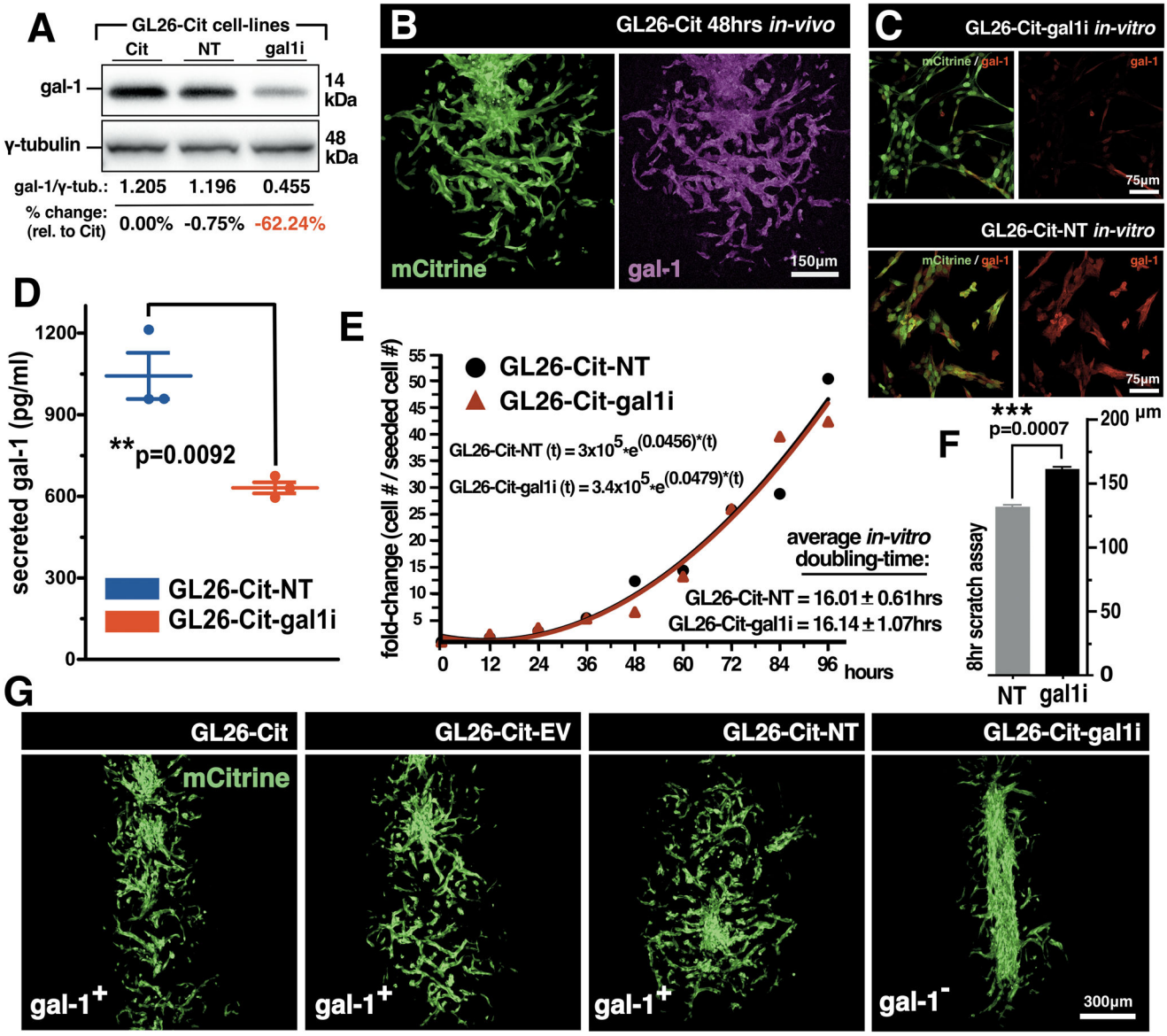

Figure 1. Gal-1 Knockdown in mouse GL26-Cit glioma cells

(A) Western blot for gal-1 in mouse GL26-Cit glioma. GL26-Cit (Cit); GL26-Cit-NT (NT); GL26-Cit-gal1i (gal1i). (B) Confocal micrograph of GL26-Cit glioma immunolabeled with gal-1 antibodies (magenta) after 48hrs in the RAG1$^{-/-}$ mouse striatum. (C) Immunocytochemistry for gal-1 in GL26-Cit-gal1i cells and GL26-Cit-NT cells. (D) Secreted gal-1 ELISA on GL26-Cit-NT and GL26-Cit-gal1i cells *in-vitro* (**p=0.0092; 1,043 ± 84.92pg/ml NT vs. 631.0 ± 20.30pg/ml gal1i; unpaired, two-tailed, Student's t-test). (E) Cell growth curve used to calculate average *in-vitro* cell doubling-times for GL26-Cit-NT and GL26-Cit-gal1i cells over 96hrs *in-vitro*. Exponential growth fitting [$r(t)=r_0ekt$] was applied to estimate respective population doubling-times as indicated. (F) Scratch assay assessing the migration rate of GL26-Cit-gal1i cells compared to GL26-Cit-NT *in-vitro* over 8hrs. (***p=0.0007; 130.58 ± 0.92μm NT vs. 161.49 ± 1.32μm gal1i; paired, two-tailed,

Student’s t-test). (G) Confocal micrographs of GL26-Cit tumors 48hrs post-tumor implantation into the RAG1$^{-/-}$ striatum.

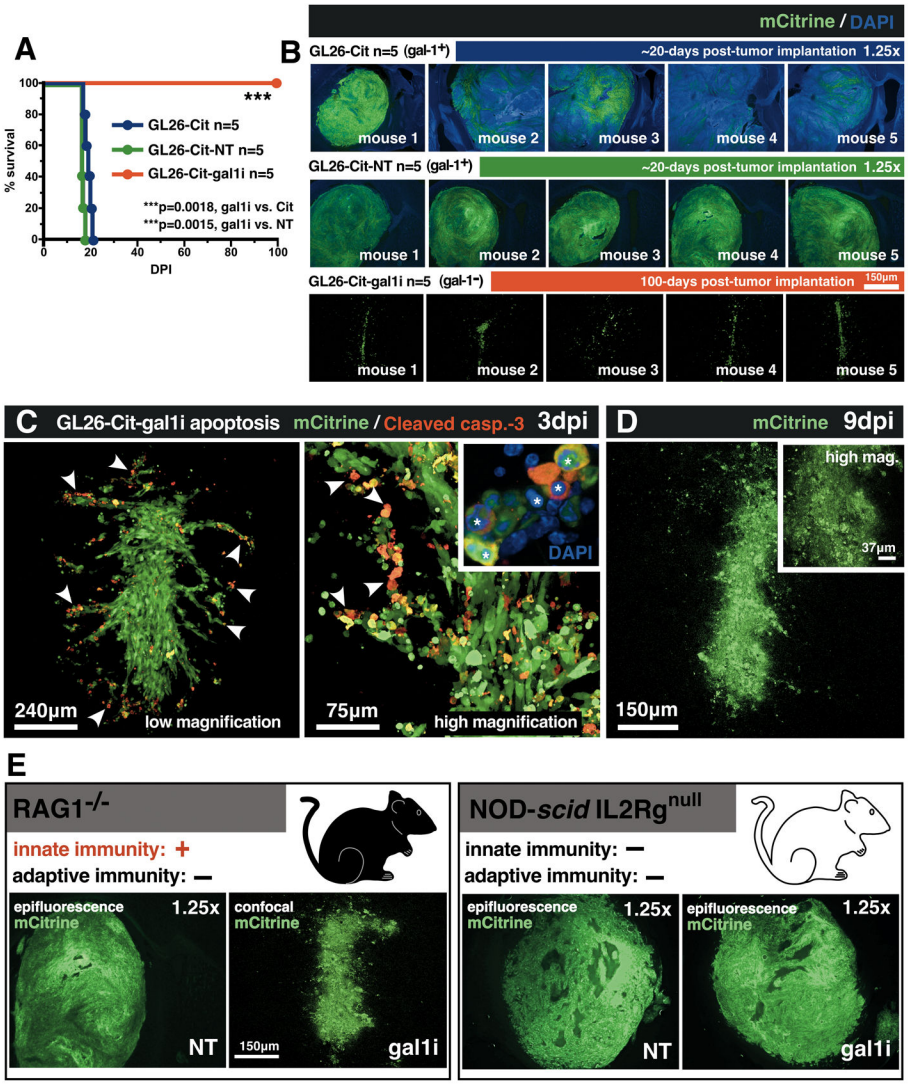

Figure 2. Gal-1 deficient glioma cells undergo early caspase-3-dependent cell-death *in-vivo*

(A) Kaplan-Meier survival analysis of RAG1$^{-/-}$ mice bearing the indicated intracranial GL26-Cit gliomas (n=45; 5 mice/group, study repeated ×3). Mantel-Cox log-rank test detected a highly significant survival difference between GL26-Cit-gal1i and both GL26-Cit (***p=0.0018) and GL26-Cit-NT (***p=0.0015) groups. (B) Epifluorescence micrographs of intracranial gliomas (green) corresponding to moribund mice from the survival analysis shown in panel A. Residual mCitrine from GL26-Cit-gal1i tumors (bottom row) 100 days post-tumor implantation (dpi) was imaged with high-magnification confocal microscopy. (C) Confocal micrographs of GL26-Cit-gal1i tumors immunolabled with anti-cleaved caspase-3 after 3dpi in the RAG1$^{-/-}$ mouse striatum. Condensed/fragmented nuclear chromatin (white asterisks) was visualized with DAPI (blue). White arrowheads indicate several examples of GL26-Cit-gal1i apoptosis. (D) Confocal micrograph of GL26-Cit-gal1i glioma after complete lysis 9dpi. (E) Representative micrographs of GL26-Cit-NT and GL26-Cit-gal1i gliomas in RAG1$^{-/-}$ and NOD-*scid* IL2Rg^{null} mice.

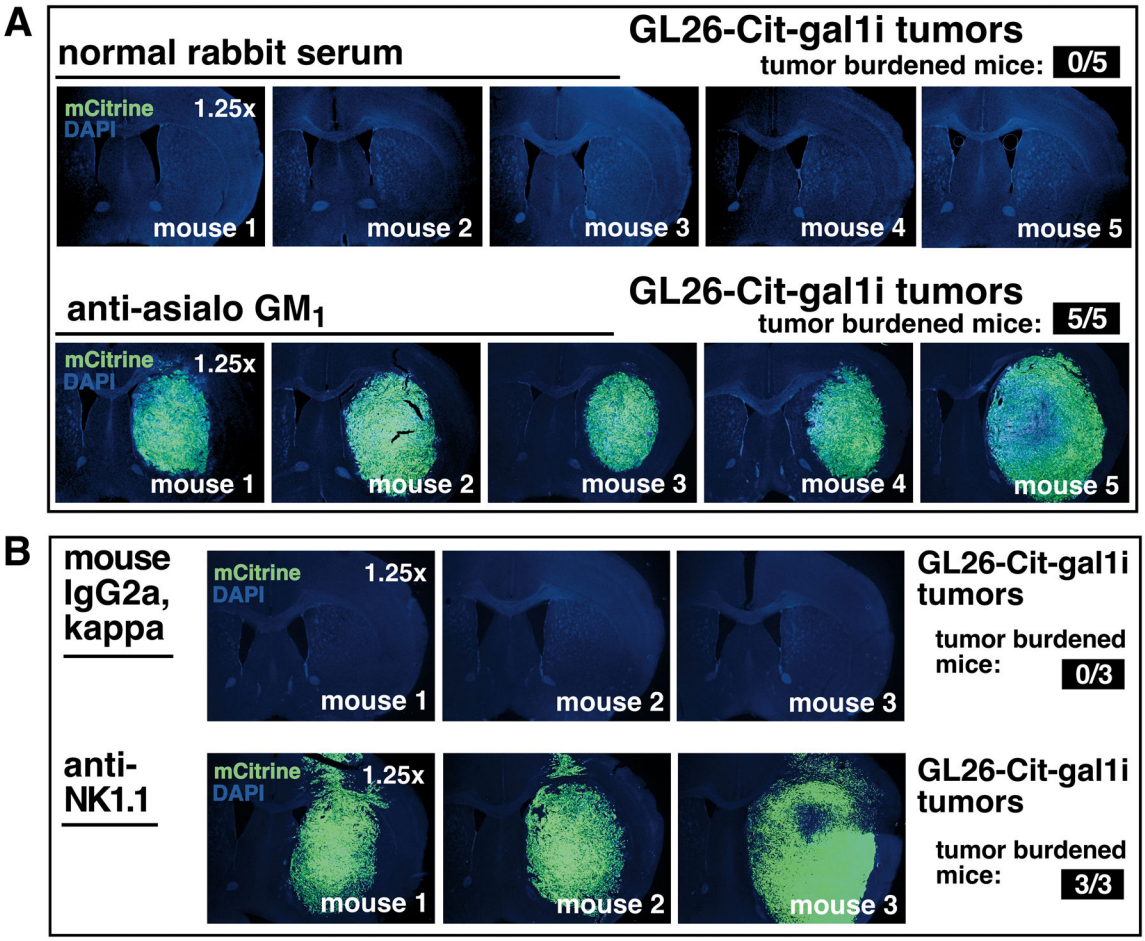

Figure 3. Immunodepletion of NK cells permits gal-1 deficient glioma growth in RAG1$^{-/-}$ mice

(A) NK cell depletion with anti-asialo GM_1 in RAG1$^{-/-}$ mice bearing GL26-Cit-gal1i cells after 16dpi. Top epifluorescence micrographs show the brains of 5 control mice. Bottom epifluorescence micrographs show the brains of 5 mice treated with NK-depleting anti-asialo GM_1 (n=20; 5 mice/treatment group; study repeated ×2; results from one study shown). (B) NK cell depletion with anti-NK1.1 monoclonal antibodies in RAG1$^{-/-}$ mice bearing GL26-Cit-gal1i cells after 16dpi. Top epifluorescence micrographs show the brains of 3 control mice. Bottom epifluorescence micrographs show the brains of 3 mice treated with anti-NK1.1 (n=6; 3mice/treatment group).

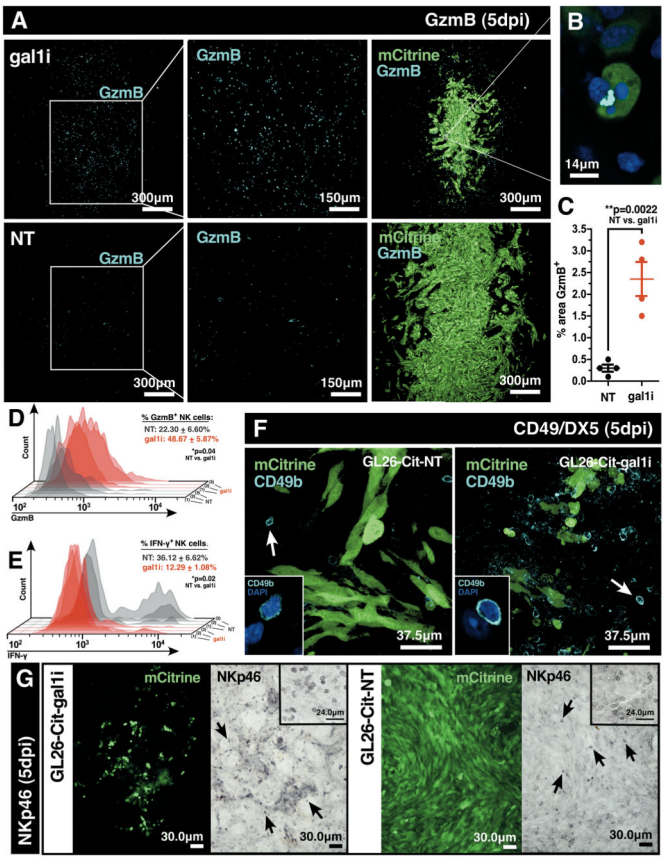

Figure 4. Gal-1 deficient gliomas are infiltrated with granzyme B$^+$ NK cells

(A) Immunofluorescence with anti-granzyme B (GzmB) antibodies on RAG1$^{-/-}$ mouse brain tissue sections bearing GL26-Cit-gal1i or GL26-Cit-NT gliomas 5dpi. (B) High-power image of an apoptotic GL26-Cit-gal1i cell associated with an accumulation of GzmB. (C) Percent area covered by GzmB immunolabeling from 20 distinct 10× brightfield micrographs using ImageJ analytical software. GL26-Cit-gal1i tumors contain significantly more immunopositive GzmB labeling (**p=0.0022; 2.35 ± 0.39% gal1i vs. 0.30 ± 0.08% GL26-Cit-NT; unpaired, two-tailed, Student's t-test). (D and E) Flow cytometric analysis of tumor-infiltrating NK cells from the cerebral hemisphere ipsilateral to the tumor implant in RAG1$^{-/-}$ mice implanted with GL26-Cit-NT (grey histograms) or GL26-Cit-gal1i (red histograms) cells (n=6; 3 mice/group) after 5dpi. (D) GL26-Cit-gal1i gliomas (red bar) contain significantly more GzmB$^+$ NK cells (*p=0.04; 48.67 ± 5.87% gal1i vs. 22.30 ± 6.60% NT; unpaired, two-tailed, Student's t-test) compared to GL26-Cit-NT gliomas (grey bar). (E) GL26-Cit-NT gliomas (grey bar) contain only few NK cells which are significantly more IFN-γ$^+$ (*p=0.02; 36.12 ± 6.62% NT vs. 12.29 ± 1.08% gal1i; unpaired, two-tailed, Student's t-test) compared to NK cells in GL26-Cit-gal1i gliomas (red bar). (F) Immunofluorescence with anti-CD49b/DX5 antibodies on RAG1$^{-/-}$ mouse brain tissue sections bearing GL26-Cit-NT or GL26-Cit-gal1i gliomas 5dpi. White arrows point to examples of CD49b/DX5$^+$ NK cells shown at higher power in the insets. (G) DAB/peroxidase immunohistochemistry with anti-NKp46 antibodies on RAG1 $^{-/-}$ mouse brain

tissue sections bearing GL26-Cit-gal1i or GL26-Cit-NT gliomas 5dpi. Black arrows point to examples of $NKp46^{+}$ NK cells. Insets provide alternative images at higher power.

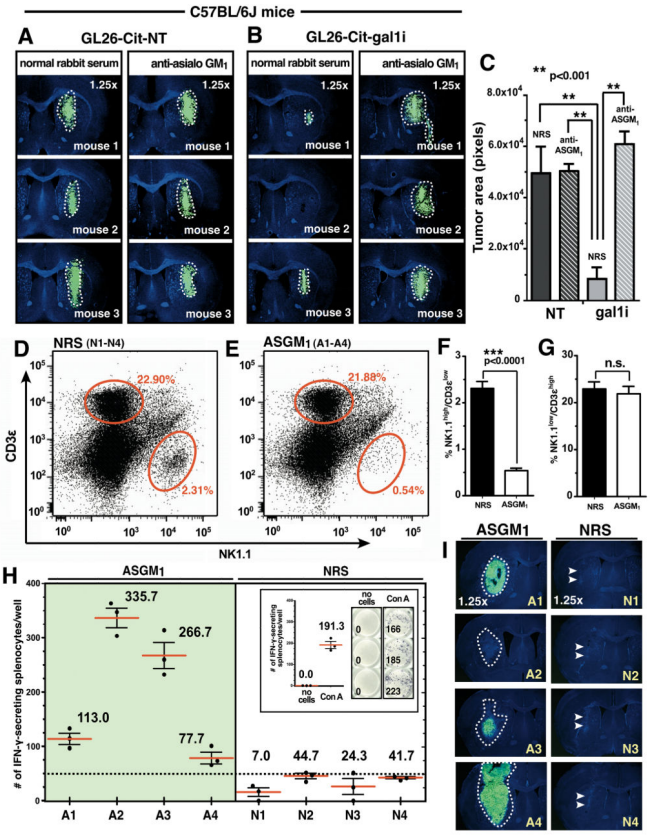

Figure 5. Gal-1 deficient glioma rejection occurs prior to the onset of antigen-specific adaptive immunity in fully immunocompetent mice

(A and B) GL26-Cit-NT and GL26-Cit-gal1i cells within the C57BL/6J striatum treated with normal rabbit serum or anti-asialo GM_1 after 5dpi. (C) Quantification of tumor areas shown throughout panels A and B using ImageJ analytical software. GL26-Cit-gal1i tumors treated with normal rabbit serum (NRS) exhibited significantly smaller tumors compared to all other groups (**p<0.001 vs. gal1i treated with NRS; one-way ANOVA followed by Tukey's post-test). (D and E) Flow cytometric plots of splenocytes immunolabeled with anti-NK1.1 and anti-CD3 ε from C57BL/6J mice bearing GL26-Cit-gal1i gliomas treated with NRS (D) or $ASGM_1$ (E) for 16dpi of (n=4 mice/treatment group, merged data shown). Average percentages of $NK1.1^{high}/CD3\ \varepsilon^{low}$ (i.e. NK cells) and $NK1.1^{low}/CD3\ \varepsilon^{high}$ (i.e. T-cells) in each treatment group are indicated by the respective red ovals. $ASGM_1$ treated leads to a significant reduction in NK cells (***p<0.0001; 2.31 ± 0.15 NRS vs. 0.54 ± 0.05 $ASGM_1$; unpaired, two-tailed, Student's t-test) while leaving T-cells unaffected (n.s., p>0.05; 22.90 ± 1.51 NRS vs. 21.88 ± 1.58 $ASGM_1$; unpaired, two-tailed, Student's t-test) (F and G respectively). (H) Tumor antigen-induced mouse IFN-γ ELISpot data. Splenocytes indicated in panels D and E were used. Splenocytes from mice treated with anti-asialo GM_1 produced high numbers of IFN-γ spots, while only a nominal number of spots (<50) were produced by splenocytes from NRS treated mice. The average number of IFN-γ spots from 3 technical replicates are shown for each mouse (red bars). Positive-(Con-A) and negative-(no splenocyte) controls are shown (inset). (I) GL26-Cit-gal1i brain tumors after 16dpi corresponding to the animals indicated in panels D-H. Glioma growth (white dashed

outlines) is seen in each $ASGM_1$ treated mouse at various stages of tumor rejection. Conversely, only a scar at the site of the initial tumor implantation (double white arrow heads) is seen in each of the NRS treated mice.

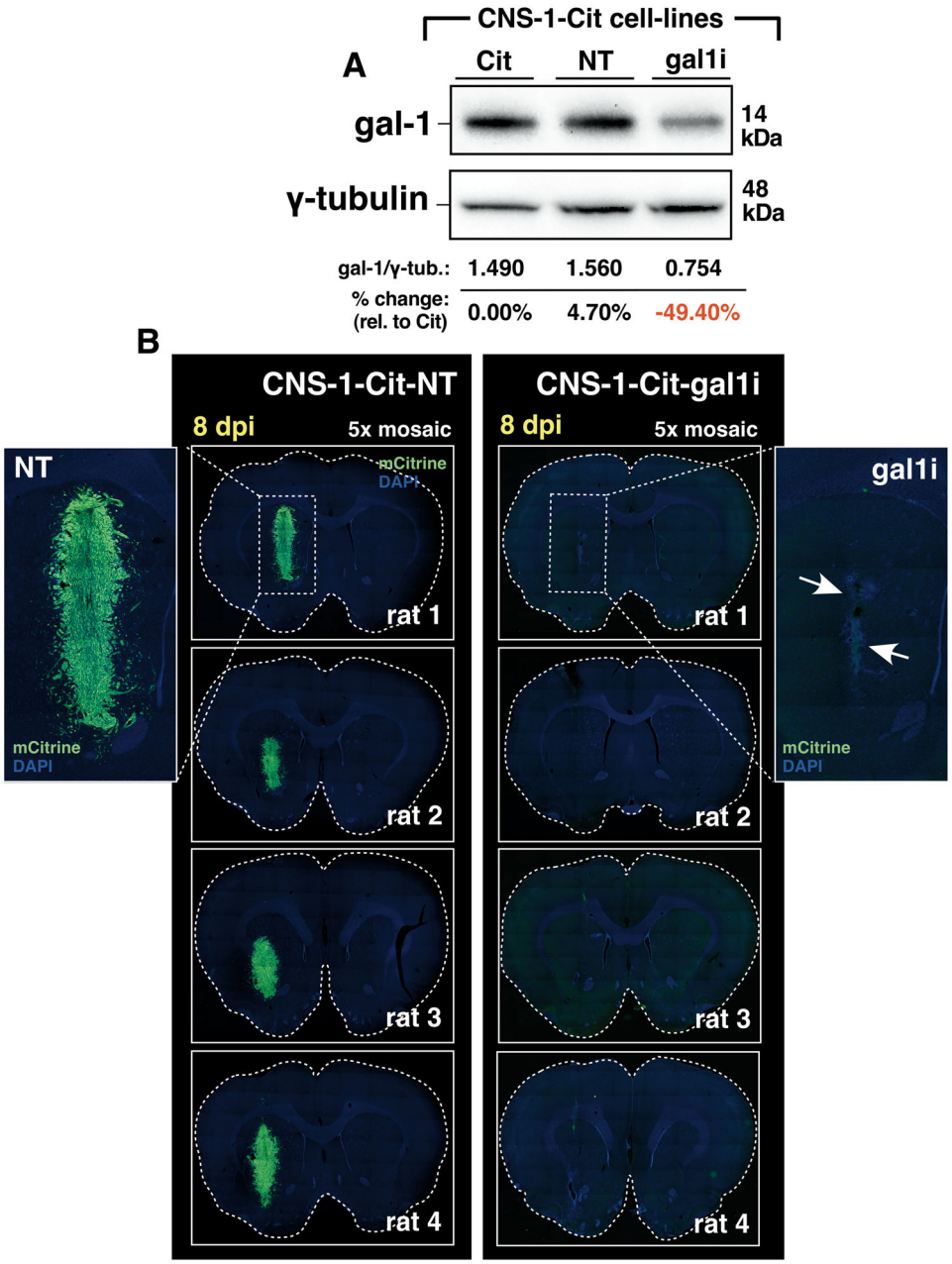

Figure 6. Gal-1 deficient rat CNS-1-Cit glioma cells fail to form intracranial tumors in syngeneic Lewis rats

(A) Western blot for gal-1 in rat CNS-1-Cit glioma. CNS-1-Cit (Cit); CNS-1-Cit-NT (NT); CNS-1-Cit-gal1i (gal1i). (B) Dual-channel epifluorescence 5× mosaic microscopy of Lewis rat brain sections bearing CNS-1-Cit-NT or CNS-1-Cit-gal1i 8dpi. Dashed white boxes in the top two micrographs are shown at higher magnification for clarity. White arrows in the GL26-Cit-gal1i example point to the non-viable tumor remnant.

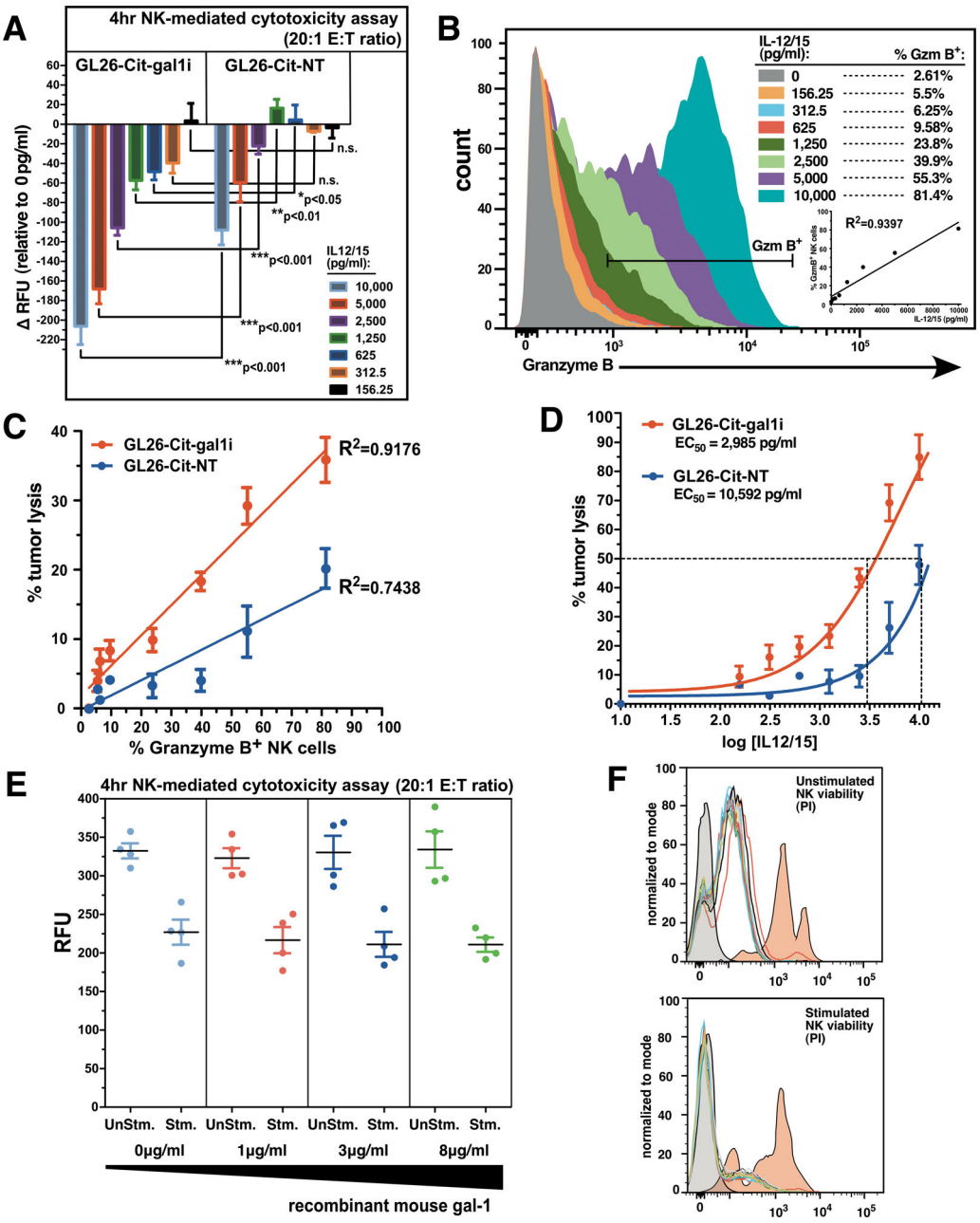

Figure 7. Gal-1 deficient glioma cells are sensitized to NK-mediated tumor lysis

(A) Change in fluorescence intensity signals (ΔRFU) from GL26-Cit-gal1i or GL26-Cit-NT cells after 4hr co-incubation with splenic-derived RAG1$^{-/-}$ NK cells stimulated overnight with the indicated concentrations of IL-12/15. GL26-Cit-gal1i cells lysed more readily in response to NK cells stimulated with all IL-12/15 concentrations above 312.5pg/ml (*p<0.05 vs. GL26-Cit-NT; two-way ANOVA). (B) Flow cytometric analysis for GzmB$^+$ NK cells after overnight culture in increasing concentrations of IL-12/15. Linear regression analysis comparing IL-12/15 concentration with % GzmB$^+$ NK cells (R^2=0.9397). (C) Linear regression analysis comparing the percentage of GzmB$^+$ NK cells and % tumor cells lysis in GL26-Cit-gal1i cells and GL26-Cit-NT cells. (D) Sigmoidal dose-response curve

fitting of log-transformed IL-12/15 concentration vs. % tumor lysis. Calculated EC_{50}'s for NK-mediated cytotoxicity are shown. (E) 4hr NK-mediated cytotoxicity assay using splenic-derived NK cells from C57BL/6J mice targeting GL26-Cit-gal1i cells at a 20:1 E:T ratio. The presence of increasing concentrations of recombinant mouse gal-1 protein fails to inhibit NK-mediated tumor lysis in response to stimulation with 10,000pg/ml IL-12/15 (n=3 wells/group). (F) Propidium iodide (PI) NK viability assay on stimulated or unstimulated NK cells in the presence of recombinant mouse gal-1 protein. Increasing concentrations of recombinant gal-1 protein fails to induce apoptosis in both NK populations. Unstained negative control (grey histograms) and staurosporine-treated positive control (red histograms) are shown.